Graphene

DOI: 10.1002/anie.201200413

Visualizing Chemical Reactions Confined under Graphene**

Rentao Mu, Qiang Fu, Li Jin, Liang Yu, Guangzong Fang, Dali Tan, and Xinhe Bao**

Reactions occurring in nanosized space often present new and extraordinary behaviors due to the nanoconfinement effect.[1–3] Understanding of the reaction mechanism relies heavily on the real-time imaging of the reactions with spatial information at the microscopic level. Although studies of surface reactions at the single-molecular-layer or even single-molecule level are feasible at open surfaces,[4–6] imaging reactions within a confined environment remains challenging. Herein, we show that interfacial reactions under graphene can be directly observed using in situ surface imaging techniques. Our results demonstrate that the graphene sheet can function as an imaging agent for reactions under its cover and, furthermore, tune the interfacial reactions.

Although two-dimensional (2D) graphene has attracted tremendous interest in the fields of physics and materials science,[7–9] the chemistry of graphene is much less explored, especially when compared to its allotrope of 1D carbon nanotubes (CNTs).[2,10] The hollow structure of the CNTs provides a confined environment for catalysts and reactants and serves as a nanoreactor.[2,11,12] Due to the tubular structure, it is difficult to probe the reactions occurring inside CNTs. Graphene as a planar material can open up a new avenue for studying surface chemistry in a confined space. The distance between graphene and substrate typically falls within 1 nm,[13] and, thus, adsorbates trapped in the small space may present novel physical and chemical properties. Moreover, dynamic processes occurring at the interface are reflected through changes in the graphene surface, thereby allowing both spectroscopic and microscopic studies of interfacial reactions.[14–16] Herein, reactions of CO confined between Pt and graphene are studied by real-time low-energy electron microscopy (LEEM)/photoemission electron microscopy (PEEM) and in situ X-ray photoelectron spectroscopy (XPS). The effect of the graphene cover on the surface chemistry of CO on Pt is also discussed.

Single-layer graphene islands were grown on a Pt(111) surface by the surface segregation process, to form single-crystalline graphene domains of micrometer size (Figure 1 and Figure S1 in the Supporting Information).[13] Inside the graphene islands, large-scale wrinkles were identified by LEEM (as marked in Figure 1 a and Figure S1). The formation of these hollow nanostructures is attributed to the different thermal expansion of Pt substrate and graphene. Upon cooling, the compressive stress built up within the graphene layer is relieved through the formation of curved carbon structures, for example, 0D nanobubbles[17] and 1D wrinkles.[13,18,19]

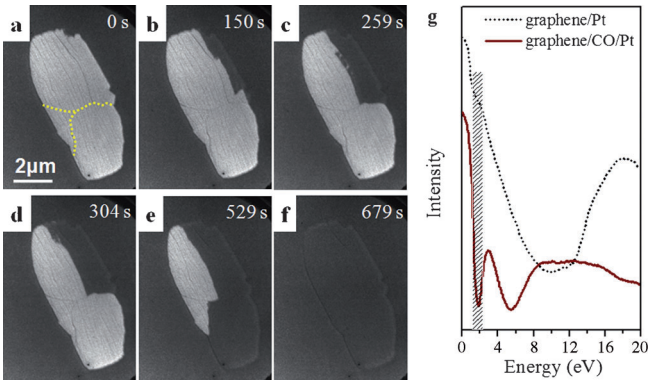

Figure 1. a–f) Series of LEEM images recorded from a single-layer graphene island on Pt(111) exposed to 1×10^{-6} mbar CO at room temperature (starting voltage, STV = 1.8 V). Wrinkles are marked with dashed lines in (a). g) Dependence of diffraction electron intensity on incident electron energy.

Exposure of CO to the graphene/Pt(111) surface was carried out at room temperature. We observed a contrast change in the LEEM images of the graphene islands when the partial pressure of CO (pCO) was raised to 1×10^{-6} mbar, which suggests the onset of CO intercalation. Figure 1 a–f displays a series of snapshots from a LEEM video recording the CO intercalation under a micrometer-sized graphene island (see Figure S2 in the Supporting Information). The real-time results show that the image contrast of the graphene island changes gradually across substrate terraces until the whole island turns dark. In contrast, no obvious change was observed under the same pCO when the Pt(111) surface was fully covered by graphene overlayers (see Figure S3 in the Supporting Information). Therefore, CO intercalation should take place through open channels at island edges, similar to our findings for the intercalation of Pb and O atoms at graphene/Ru(0001) interfaces.[20–22]

The distance between graphene and the Pt(111) substrate was measured to be around 3.30 Å.[13,23] Considering the CO molecule has a kinetic diameter of 3.76 Å,[24] CO intercalation should enlarge the distance between the graphene sheet and the Pt surface, thus leading to a change in the intensity of diffraction electrons.[25] To demonstrate this, we measured the diffraction intensity as a function of the incident beam energy (*I–V* curves) from the graphene/Pt(111) surface and the CO-

[*] R. T. Mu, Prof. Q. Fu, L. Jin, L. Yu, G. Z. Fang, D. L. Tan, Prof. X. H. Bao
State Key Laboratory of Catalysis,
Dalian Institute of Chemical Physics
Zhongshan Road 457, Dalian 116023 (P.R. China)
E-mail: qfu@dicp.ac.cn
xhbao@dicp.ac.cn

[**] This work was supported by the Ministry of Science and Technology of China (MOST, No. 2011CB932704), the Natural Science Foundation of China (NSFC, Nos. 21073183, 21033009, and 11079005), and the Chinese Academy of Sciences (CAS). We acknowledge the fruitful discussion with Weixue Li and Fan Yang.

Supporting information for this article is available on the WWW under http://dx.doi.org/10.1002/anie.201200413.

intercalated graphene surface. As shown in Figure 1 g, the *I–V* curve taken from the CO-intercalated surface presents two local intensity minima at 1.8 and 5.4 eV. Since the LEEM images were taken at the starting voltage (STV) of approximately 1.8 V, the diffraction intensity from the CO-intercalated graphene surface is much lower than that from the graphene/Pt(111) surface, which suggests the main mechanism of imaging the CO intercalation by LEEM.

Microregion low-energy electron diffraction (μ-LEED) further shows that the Moiré pattern,[13] which is due to the interaction between graphene and Pt(111) (Figure 2 a), dis-

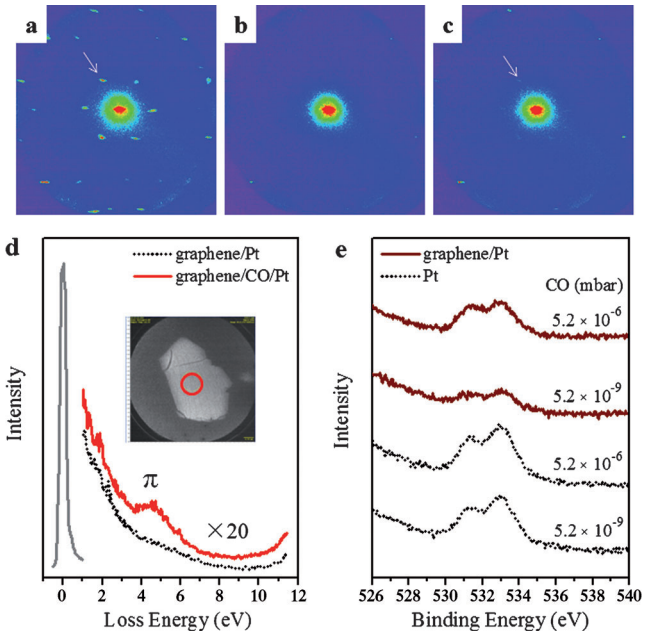

Figure 2. a–c) μ-LEED patterns from a) the graphene/Pt(111) surface in ultrahigh vacuum (UHV), b) the CO-intercalated graphene kept in a CO atmosphere, and c) the graphene/CO/Pt(111) surface kept in UHV and at room temperature. The arrows mark the satellite spots due to the Moiré structures of graphene. d) Spatially resolved EELS spectra from a graphene island on Pt(111) before and after the CO intercalation reaction. The circle in the inset indicates the analysis area. e) XPS O 1s spectra from Pt(111) and 0.7 ML graphene/Pt(111) surfaces saturated at 5.2×10^{-9} and 5.2×10^{-6} mbar CO, respectively, at room temperature.

appears upon CO intercalation (Figure 2 b). The removal of the Moiré structure indicates that the interaction is decoupled by the CO intercalation. The electronic structure of graphene islands was studied using spatially resolved electron energy loss spectroscopy (EELS) in the LEEM instrument[26] (Figure 2 d). It has been shown that the collective excitation of π electrons in the freestanding graphene causes a characteristic loss feature between 4 and 7 eV.[26,27] On the graphene/Pt(111) surface, such a feature cannot be observed because the π-band structure becomes disrupted by electronic interaction between graphene islands and the Pt substrate. In contrast, EELS from the CO-intercalated graphene surface displays the characteristic feature located at 4.8 eV. Both μ-LEED and EELS measurements confirm that CO molecules penetrate into the graphene/Pt(111) interface and decouple the graphene layer from the substrate.

The CO intercalation was also studied by using in situ XPS. Figure 2 e shows that the saturation coverage of CO remains constant on Pt(111) at the pCO range between 5.2×10^{-9} and 5.2×10^{-6} mbar. In comparison, the saturation coverage of CO on the 0.7 monolayer (ML) graphene/Pt(111) surface is only about 31 % of that on bare Pt(111) after exposure to 5.2×10^{-9} mbar CO. When the graphene/Pt(111) surface was exposed to 5.2×10^{-6} mbar CO, XPS measurement taken in 5.2×10^{-8} mbar CO indicates that the surface coverage of CO is about three times that of the value upon exposure to 5.2×10^{-9} mbar CO. This is consistent with the LEEM results (Figure 1), and shows that CO intercalation starts with pCO above 1×10^{-6} mbar. Based on XPS measurements, the CO density under the graphene cover is approximately 80 % of that on the bare Pt(111) surface.

On the CO-covered Pt(111) surface, O 1s spectra contain two peaks at 533.0 and 531.3 eV, corresponding to CO adsorption at the top site (t-CO) and bridge site (b-CO) of Pt(111), respectively.[28] The ratio of O 1s intensity from b-CO and t-CO ($I_{b\text{-}CO}/I_{t\text{-}CO}$) is 1:1.9. In contrast, $I_{b\text{-}CO}/I_{t\text{-}CO}$ increases to 1:1.2 on the graphene/CO/Pt(111) surface, which suggests that t-CO becomes less favorable under graphene because of the higher steric position of t-CO than b-CO.

Once CO gas is removed from the chamber, real-time LEEM/laser-PEEM images reveal that the molecules confined under the graphene start to desorb even at room temperature (Figure 3 a–c and Figures S4 and S5 in the

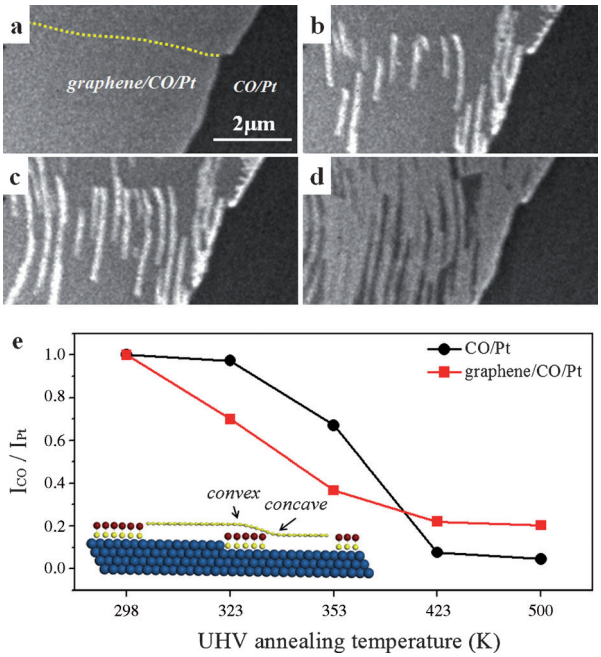

Figure 3. a–c) LEEM images from the graphene/CO/Pt(111) surface kept in UHV and at room temperature for different times: a) 0, b) 200, c) 402 s. d) Further annealing at 487 K in UHV. STV = 2.4 V. The dashed line in (a) marks the wrinkle location. e) XPS O 1s intensity of the CO-saturated Pt(111) surface and the CO-intercalated 0.7 ML graphene/Pt(111) surface annealed at various temperatures in UHV. The O 1s intensity was normalized by the Pt 4f intensity. Each annealing step lasted more than 10 min. The inset illustrates desorption of CO molecules under graphene, except those trapped close to steps, at around room temperature.

Supporting Information). It is found that CO desorption is initiated at the terrace sites close to the wrinkles and develops simultaneously at many terraces. The wrinkle acts as a nanosized outlet for CO desorption. In addition, the weak Moiré pattern of the graphene appears again in μ-LEED after pumping away CO (Figure 2c). The interaction between graphene and Pt was partially recovered when some of the CO molecules below the graphene desorbed.

XPS studies also show that the O 1s intensity decreases by 30% when the CO-intercalated surface is kept at 323 K and in UHV. After annealing the graphene/CO/Pt(111) surface at 423 K, there is still 20% of full CO coverage (Figure 3e), which does not change after annealing at 500 K. For comparison, the same desorption procedure was applied to the CO-saturated Pt(111) surface. The O 1s intensity remains constant at 323 K, while CO desorbs completely above 423 K (Figure 3e), similar to our previous results.[29]

Both LEEM/PEEM and XPS experiments demonstrate that the majority of intercalated CO molecules are destabilized on Pt surface terraces covered by graphene, which can desorb even around room temperature. The earlier desorption of O atoms from the graphene/Ru(0001) interface than from the bare Ru(0001) surface was also reported previously by us.[20] Nevertheless, the present observations are still quite surprising since CO is known to poison Pt surfaces and hardly desorbs at room temperature.[30]

To obtain a tentative explanation for the effect of the graphene cover on CO adsorption, we conducted density functional theory (DFT) calculations of CO adsorption energies (E_{ad}) at various graphene–Pt(111) distances ($D_{graphene-Pt}$; see Figure S6 in the Supporting Information). At the equilibrium state of fully relaxed graphene, $D_{graphene-Pt}$ with CO adsorbed at the top site is 5.91 Å. Shrinking the $D_{graphene-Pt}$ owing to the graphene–metal interaction leads to smaller CO adsorption energy (see Figure S6 in the Supporting Information). For example, E_{ad} of t-CO decreases by 0.4 eV as the $D_{graphene-Pt}$ value falls to 5.3 Å. The calculations confirm that CO adsorption on Pt(111) is weakened by the presence of the graphene cover. The smaller the nanospace, the weaker the CO adsorption.

On the other hand, we do observe that a small portion of the intercalated CO molecules remains trapped close to the steps, which can be stable on the surface even above 500 K (Figure 3d,e). When placing an atomically continuous carbon sheet on a stepped metal surface, carbon atoms close to the lower and upper edges of each step become distorted from a planar structure, forming concave and convex regions with nanometer width (inset of Figure 3e).[31] These carbon atoms interact strongly with the metal surface,[32] and function as barriers for outward diffusion of CO to desorb. Thus, rows of CO molecules close to the steps can be geometrically trapped between the concave and convex graphene regions. The confined CO molecules form 1D columns near the steps (graphene/1D-CO/Pt(111) surface). With the aid of the monolayer graphene cover, reaction of the confined CO molecules with O_2 (1.3×10^{-6} mbar O_2, 493 K) below the graphene can be visualized by LEEM (Figure 4a,b, and see Video S7 in the Supporting Information). The reaction starts from the wrinkles and proceeds along the steps. Again, the

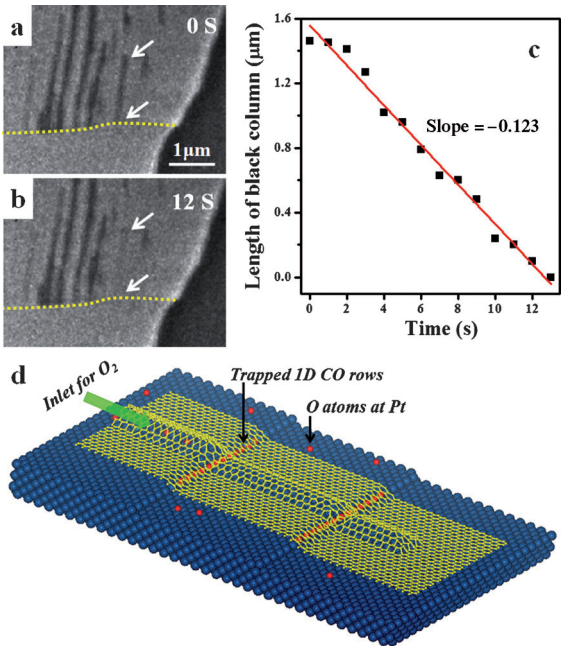

Figure 4. a, b) LEEM images of the CO oxidation process. Graphene/1D-CO/Pt(111) exposed to 1.3×10^{-6} mbar O_2 at 493 K for 12 s; STV = 2.4 eV. Dashed lines mark the wrinkle. c) Plot of the length of the 1D CO molecular column as a function of reaction time. d) Schematic showing a reaction under the graphene cover with a wrinkle structure. Pt cyan, C yellow, O red. The wrinkle functions as a nanosized inlet/outlet for molecules such as O_2.

wrinkle functions as a nanosized inlet for O_2 to react with the trapped CO molecules close to the steps (Figure 4d). As shown in Figure 4c, the reaction rate r can be determined as $r = (\theta dL)/(2r_{Pt}dt) = 177$ molecule s^{-1}, where θ is the coverage of CO at the graphene/Pt interface, r_{Pt} is the radius of the Pt atom, L is the column length and t is time.

In summary, graphene has manifested itself as an imaging agent to visualize interfacial reactions under its cover. It has been directly imaged that CO penetrates into the graphene/Pt(111) interface at room temperature with pCO in the range of 10^{-6} mbar, whereas the intercalated CO can desorb from the Pt surface around room temperature and in UHV. Furthermore, the reaction process of CO oxidation confined at the graphene/Pt interface can be seen as well. Our findings reveal that the graphene layer exhibits a strong confinement effect on the chemistry of molecules underneath. The 2D nanospace under graphene provides an intriguing confinement environment for surface chemistry and catalysis.

Experimental Section

In situ microscopic studies were carried out in an Elmitec LEEM/PEEM system, which contained a preparation chamber, an imaging system, and a vacuum ultraviolet (VUV) laser source ($\lambda = 177.3$ nm) for PEEM.[21] Graphene layers were grown on Pt(111) by chemical vapor deposition (CVD), that is, exposure of the Pt(111) surface to 1.3×10^{-7} mbar ethylene at 950 K, or by surface segregation at 900–950 K and in UHV. High-purity gases, such as CO and O_2, were introduced into the surface by backfilling the chamber with a partial pressure up to 5×10^{-6} mbar.

In situ spectroscopic measurements were performed in an Omicron multiprobe system, equipped for XPS, ultraviolet photoelectron spectroscopy, and scanning tunneling microscopy.[20] In this system, graphene was deposited on the Pt(111) surface by CVD. The coverage of the graphene layers was calibrated by measuring the XPS C 1s intensity and performing CO titration. The intercalation of CO at the graphene/Pt(111) surface was performed at room temperature and with pCO between 5.2×10^{-9} and 5.2×10^{-6} mbar. In situ XPS measurements were carried out with pCO below 5.2×10^{-8} mbar.

Calculations were performed using the Vienna Ab Initio Simulation Package (VASP) with the projector-augmented wave method and a cutoff energy of 400 eV.[33] The graphene/Pt model was constructed in supercells with 3×3 graphene on a $(\sqrt{7}\times\sqrt{7})$ four-layer slab of Pt(111) (for details, see Figure S6 in the Supporting Information).

Received: January 16, 2012
Revised: March 2, 2012
Published online: April 11, 2012

Keywords: CO oxidation · graphene · imaging agents · interfaces · surface chemistry

[1] J. M. Thomas, R. Raja, *Acc. Chem. Res.* **2008**, *41*, 708 – 720.
[2] X. L. Pan, X. H. Bao, *Acc. Chem. Res.* **2011**, *44*, 553 – 562.
[3] B. Smit, T. L. M. Maesen, *Nature* **2008**, *451*, 671 – 678.
[4] M. Kim, M. Bertram, M. Pollmann, A. von Oertzen, A. S. Mikhailov, H. H. Rotermund, G. Ertl, *Science* **2001**, *292*, 1357 – 1360.
[5] B. Hulsken, R. Van Hameren, J. W. Gerritsen, T. Khoury, P. Thordarson, M. J. Crossley, A. E. Rowan, R. J. M. Nolte, J. A. A. W. Elemans, S. Speller, *Nat. Nanotechnol.* **2007**, *2*, 285 – 289.
[6] S. Katano, Y. Kim, M. Hori, M. Trenary, M. Kawai, *Science* **2007**, *316*, 1883 – 1886.
[7] K. S. Novoselov, A. K. Geim, S. V. Morozov, D. Jiang, Y. Zhang, S. V. Dubonos, I. V. Grigorieva, A. A. Firsov, *Science* **2004**, *306*, 666 – 669.
[8] Y. B. Zhang, Y. W. Tan, H. L. Stormer, P. Kim, *Nature* **2005**, *438*, 201 – 204.
[9] A. K. Geim, K. S. Novoselov, *Nat. Mater.* **2007**, *6*, 183 – 191.
[10] R. Ruoff, *Nat. Nanotechnol.* **2008**, *3*, 10 – 11.
[11] X. L. Pan, Z. L. Fan, W. Chen, Y. J. Ding, H. Y. Luo, X. H. Bao, *Nat. Mater.* **2007**, *6*, 507 – 511.
[12] E. Castillejos, P. J. Debouttiere, L. Roiban, A. Solhy, V. Martinez, Y. Kihn, O. Ersen, K. Philippot, B. Chaudret, P. Serp, *Angew. Chem.* **2009**, *121*, 2567 – 2571; *Angew. Chem. Int. Ed.* **2009**, *48*, 2529 – 2533.
[13] P. Sutter, J. T. Sadowski, E. Sutter, *Phys. Rev. B* **2009**, *80*, 245411.
[14] A. Varykhalov, W. Gudat, O. Rader, *Adv. Mater.* **2010**, *22*, 3307 – 3310.
[15] K. Xu, P. G. Cao, J. R. Heath, *Science* **2010**, *329*, 1188 – 1191.
[16] P. Sutter, J. T. Sadowski, E. A. Sutter, *J. Am. Chem. Soc.* **2010**, *132*, 8175 – 8179.
[17] N. Levy, S. A. Burke, K. L. Meaker, M. Panlasigui, A. Zettl, F. Guinea, A. H. C. Neto, M. F. Crommie, *Science* **2010**, *329*, 544 – 547.
[18] A. T. N′Diaye, R. van Gastel, A. J. Martinez-Galera, J. Coraux, H. Hattab, D. Wall, F. J. M. zu Heringdorf, M. Horn-von Hoegen, J. M. Gomez-Rodriguez, B. Poelsema, C. Busse, T. Michely, *New J. Phys.* **2009**, *11*, 113056.
[19] E. Loginova, S. Nie, K. Thurmer, N. C. Bartelt, K. F. McCarty, *Phys. Rev. B* **2009**, *80*, 085430.
[20] H. Zhang, Q. Fu, Y. Cui, D. L. Tan, X. H. Bao, *J. Phys. Chem. C* **2009**, *113*, 8296 – 8301.
[21] L. Jin, Q. Fu, R. T. Mu, D. L. Tan, X. H. Bao, *Phys. Chem. Chem. Phys.* **2011**, *13*, 16655 – 16660.
[22] L. Jin, Q. Fu, H. Zhang, R. T. Mu, Y. H. Zhang, D. L. Tan, X. H. Bao, *J. Phys. Chem. C* **2012**, *116*, 2988 – 2993.
[23] M. Gao, Y. Pan, C. D. Zhang, H. Hu, R. Yang, H. L. Lu, J. M. Cai, S. X. Du, F. Liu, H. J. Gao, *Appl. Phys. Lett.* **2010**, *96*, 053109.
[24] R. W. Baker, *Membrane Technology and Applications*, *2nd ed.*, Wiley, Chichester, **2004**.
[25] V. Blum, K. Heinz, *Comput. Phys. Commun.* **2001**, *134*, 392 – 425.
[26] S. Oida, F. R. McFeely, J. B. Hannon, R. M. Tromp, M. Copel, Z. Chen, Y. Sun, D. B. Farmer, J. Yurkas, *Phys. Rev. B* **2010**, *82*, 041411.
[27] T. Eberlein, U. Bangert, R. R. Nair, R. Jones, M. Gass, A. L. Bleloch, K. S. Novoselov, A. Geim, P. R. Briddon, *Phys. Rev. B* **2008**, *77*, 233406.
[28] M. Kinne, T. Fuhrmann, J. F. Zhu, B. Trankenschuh, R. Denecke, H. P. Steinruck, *Langmuir* **2004**, *20*, 1819 – 1826.
[29] T. Ma, Q. Fu, H. Y. Su, H. Y. Liu, Y. Cui, Z. Wang, R. T. Mu, W. X. Li, X. H. Bao, *ChemPhysChem* **2009**, *10*, 1013 – 1016.
[30] Y. Y. Yeo, L. Vattuone, D. A. King, *J. Chem. Phys.* **1997**, *106*, 392 – 401.
[31] J. Coraux, A. T. N′Diaye, C. Busse, T. Michely, *Nano Lett.* **2008**, *8*, 565 – 570.
[32] P. J. Feibelman, *Phys. Rev. B* **2008**, *77*, 165419.
[33] G. Kresse, J. Hafner, *Phys. Rev. B* **1993**, *48*, 13115 – 13118.

